Advances in Materials Physics and Chemistry, 2013, 3, 133-145
http://dx.doi.org/10.4236/ampc.2013.32019 Published Online June 2013 (http://www.scirp.org/journal/ampc)

Structure, Photochromism and Liquid Crystal Properties of 1-Alkyl-2-(Arylazo)Imidazoles (Raai-C_nH_{2n+1}, n (Even) = 10 - 22)

Avijit Nandi[1], Chandana Sen[1], Debashis Mallick[2], Randhir K. Sinha[1], Chittaranjan Sinha[1*]
[1]Department of Chemistry, Inorganic Chemistry Section, Jadavpur University, Kolkata, India
[2]Department of Chemistry, Mrinalini Datta Mahavidyapith, Birati, India
Email: *c_r_sinha@yahoo.com

Received March 16, 2013; revised May 4, 2013; accepted May 18, 2013

ABSTRACT

Photochromism is the reversible structural change of the molecules upon light irradiation having different spectral pattern before and after irradiation. Liquid crystal (LC) is a long-range orientational order of the molecules in between solid and isotropic liquid phases which share the properties of the crystal and liquid phases. 1-Alkyl-2-(arylazo)imidazoles, (Raai-C_nH_{2n+1}, R = H, Me and n = 10, 12, 14, 16, 18, 20, 22) exhibits photochromism and two of them (Haai-$C_{18}H_{37}$ and Haai-$C_{22}H_{45}$) show Liquid crystal (LC) properties. One of these compounds, Meaai-$C_{16}H_{33}$ is structurally characterized by single crystal X-ray diffraction study. The compounds upon irradiation with UV light show E-to-Z isomerisation. Quantum yields ($\phi_{E\rightarrow Z}$) of E-to-Z isomerisation vary with the molar mass of the compounds. The reverse transformation, Z-to-E, is recorded in thermal condition. The activation energy (E_a) of isomerisation is determined by the controlled temperature reaction. Liquid crystal property of the molecules is examined by polarizing optical microscopy (POM) and DSC. The carbon chain length n = 18 shows nematic (N)-isotropic (I) phase transition and an unknown Smectic (Sm) phase is observed with n = 22 on heating cycle.

Keywords: Arylazoimidazoles; Structure; Photochromism; Liquid Crystal; Nematic-Isotropic Phase Transition; Smectic Phase

1. Introduction

Smart molecules can respond to a specific external stimulus in a specific manner and are of increasing interest in areas as diverse as microbiology [1], microfluidics [2], organic electronics [3,4], high density optical data storage devices [5,6] etc. Using of light as external stimulating agent has manifold advantages. Fritzsche (1867) observed the bleaching of an orange colored tetracene solution in daylight and then re-colored at night [7]. However, during the 1950s, the research groups of Hirshberg and Fischer carried out comprehensive studies on light irradiated color changes and the subsequent physical and chemical changes of different organic molecules [8]. The research field has received a renewable thrust in the 1980s when the photo-induced reversible transformation was observed for organic molecules like spirooxazines, diarylethenes etc. without photodegradation. This process is known as photochromism. It is defined as "reversible transformation of a chemical species induced in one or both directions by the absorption of electromagnetic radiation between two forms having different absorption spectra" [9]. The photochromic compounds have become appealing for their potential advantages in the construction of photo-switching devices and supramolecular architectures [9-15]. Various organic compounds show cis(Z)/trans(E) isomerization, pericyclic reactions, H atom transfer reactions, and dissociation processes. The molecules have been used as photoresponsive functional devices utilized as smart polymers [16], liquid crystals [17], molecular switches [18] and machines [19].

Azobenzene is used for a wide range of applications, from dye indicators and nonlinear optical chromophores to quantum interferences [20]. The molecule shows photoinduced E/Z isomerization by UV or visible light. More recently the synthesis and the characterization of heterocyclic azo dyes such as arylazopyridines have been extensively reported [21-24]. The prospect of azobenzene has encouraged us for synthesizing arylazoimidazoles

*Corresponding author.

[25] which acts as a potential switching group in biology and in coordination chemistry, since imidazole is a ubiquitous and essential group in biology, especially as a metal coordinating. The photochromism of 1-alkyl-2-(arylazo)imidazole (RaaiR) [26,27] and some of their complexes [28-31] are also reported.

The liquid crystal (LC) is a long-range orientational order and lies in between solid and isotropic liquid phases. The LC phase (mesophase) shares properties of the crystal and liquid phases. Some examples of anisotropic properties are birefringence, alignment in electric and magnetic fields (electrical permittivity and magnetic susceptibility), elasticity, viscosity, and conductivity [32,33]. Liquid crystals are widely used in information display technology and the anisotropic fluid states of rigid polymers are used for processing of high strength fibers. Liquid crystals (LCs) should also be useful in bio-related fields because the self-organized structures of lyotropic liquid crystals are compatible with those in living systems [34].

Comparing with azobenzene photochrome, arylazoimidazoles have several advantages of possessing both the photoactivity related to the azo unit, the capability of self-assembly through the imidazolyl group and coordinating ability to metal ions. Azoimidazoles display surprisingly a strong tendency toward self-assembly, which offers a new and efficient way to make photoactive liquid crystal (LC) materials. Attachment of long chain alkyl groups to aromatic molecules may develop liquid crystal (LC) property. The E form of azo derivatives is a rod and is nematic LCs (NLCs) while the Z is bent and tends to destabilize the phase structure. Therefore, E/Z photoisomerization of the azobenzene in the N phase can disorganize the phase structure of NLCs, resulting in a nematic-isotropic (N-I) isothermal phase transition (photochemical phase transition). In this article, we describe a preliminary account on photochromic LC (PLC) activity of some long chain alkyl group substituted 1-alkyl-2-(arylazo)imidazoles, Raai-C_nH_{2n+1} (n = 10, 12, 14, 16, 18, 20, 22).

2. Experimental

2.1. Materials

1-Alkyl-2-(arylazo)imidazoles were synthesized by reported procedure [27]. 1-Bromo-n-alkanes, n-$C_{10}H_{21}$-1-Br, n-$C_{12}H_{25}$-1-Br, $C_{14}H_{29}$-1-Br and 1-chloro-n-alkanes, $C_{16}H_{33}$-1-Cl, $C_{18}H_{37}$-1-Cl, $C_{20}H_{41}$-1-Cl and $C_{22}H_{45}$-1-Cl were purchased from Sigma-Aldrich and used as such. All other chemicals and solvents were analytical reagent grade as received.

2.2. Physical Measurements

Microanalytical data (C, H, N) were collected on Perkin-Elmer 2400 CHNS/O elemental analyzer. Spectroscopic data were obtained using the following instruments: UV-Vis spectra from a Perkin Elmer Lambda 25 spectrophotometer; IR spectra (KBr disk, 4000 - 400 cm^{-1}) from a Perkin Elmer RX-1 FTIR spectrophotometer; photo excitation has been carried out using a Perkin Elmer LS-55 spectrofluorimeter and ^1H NMR spectra were recorded from a Bruker (AC) 300 MHz FTNMR spectrometer. The liquid crystalline properties were established by thermal microscopy (Nikon polarizing microscope LV100POL attached with Linkam Temperature controlled stage model Examina-THMS600, and the phase transitions were confirmed by differential scanning calorimetry (Perkin-Elmer Diamond DSC Pyris1 system).

2.3. Synthesis of Compounds

2-(Arylazo)imidazoles were synthesized by the diazotization of aniline or *p*-toluidine in $NaNO_2$/HCl at low temperature (0˚C - 5˚C) and followed by coupling with imidazole in aqueous sodium carbonate solution (pH-7). The alkylation was carried out by adding alkyl halide in dry THF solution to the corresponding 1-alkyl-2-(arylazo) imidazole in presence of NaH (**Scheme 1**). Long chain alkyl groups are appended at imidazole motif to synthesise present series of molecules. The compounds are 1-alkyl-2-(arylazo)imidazole [Raai-C_nH_{2n+1}, where R = H (**a**), Me (**b**); C_nH_{2n+1}—where n = 10 ($C_{10}H_{21}$, **1**), 12 ($C_{12}H_{25}$, **2**), 14 ($C_{14}H_{29}$, **3**), 16 ($C_{16}H_{33}$, **4**), 18 ($C_{18}H_{37}$, **5**), 20 ($C_{20}H_{41}$, **6**), 22 ($C_{22}H_{45}$, **7**)]. Detail synthesis for Me-aai-$C_{10}H_{21}$ (**1b**) is given below.

To dry THF solution (75 ml) of 2-(*p*-tolylazo)imidazole (2 g, 10.8 mmol), NaH (50% paraffin) (0.56 g) was added in small portion and stirred at cold condition on ice bath for 0.5 h. 1-Bromodecane (n-$C_{10}H_{21}$-1-Br; 2.50 g, 11.31 mmol) in dry THF (25 ml) was added slowly through pressure equalizing system under stirring condition for a period of 1 h and then warm for another 1 h on steam bath. The solution was evaporated to dryness, extracted with CH_2Cl_2, washed with NaOH solution (10%, 10 ml × 3) and finally by distilled water (20 ml × 3). The CH_2Cl_2 extract was chromatographed over silica gel-column (45 × 1 ml) prepared in petroleum ether (40˚C - 60˚C). The elution was performed by ethylacetate-pe-

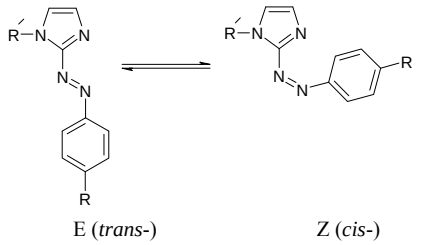

E (*trans*-) Z (*cis*-)

Scheme 1. Isomerization of 1-alkyl-2-(arylazo)imidazole.

troleum ether (1:3 v/v) mixture and evaporated under reduced pressure. An orange crystalline product was obtained and then dried over P_4O_{10} under vacuum. Yield of the product was 2.28 g (65%).

All other compounds were prepared and purified by identical procedure and the yield was varied 55% - 70%. The microanalytical data of the compounds are as follows: Haai-$C_{10}H_{21}$ (**1a**), 54˚C ± 1˚C, *Anal.* Found: C, 73.00; H, 9.00; N, 18.00 Calc. for $C_{19}H_{28}N_4$: C, 73.08; H, 8.97; N, 17.95. Meaai-$C_{10}H_{21}$ (**1b**), 53˚C ± 1˚C, *Anal.* Found: C, 73.70; H, 9.13; N, 17.23 Calc. for $C_{20}H_{30}N_4$: C, 73.62; H, 9.20; N, 17.18. Haai-$C_{12}H_{25}$ (**2a**), 54˚C ± 1˚C, *Anal.* Found: C, 74.20; H, 9.36; N, 16.40. Calc. for $C_{21}H_{32}N_4$: C, 74.12; H, 9.41; N, 16.47. Meaai-$C_{12}H_{25}$ (**2b**), 52˚C ± 1˚C, *Anal.* Found: C, 74.64; H, 9.55; N, 15.90 Calc. for $C_{22}H_{34}N_4$: C, 74.58; H, 9.60; N, 15.82. Haai-$C_{14}H_{29}$ (**3a**), 54˚C ± 1˚C, *Anal.* Found: C, 74.94; H, 9.84; N, 15.30 Calc. for $C_{23}H_{36}N_4$: C, 75.00; H, 9.78; N, 15.22. Meaai-$C_{14}H_{29}$ (**3b**), 53˚C ± 1˚C *Anal.* Found: C, 75.47; H, 9.92; N, 14.72 Calc. for $C_{24}H_{38}N_4$: C, 75.39; H, 9.95; N, 14.66. Haai-$C_{16}H_{33}$ (**4a**), 53 ± 1˚C, *Anal.* Found: C, 75.70; H, 10.05; N, 14.20 Calc. for $C_{25}H_{40}N_4$: C, 75.76; H, 10.10; N, 14.14. Meaai-$C_{16}H_{33}$ (**4b**), 54˚C ± 1˚C, *Anal.* Found: C, 76.12; H, 10.20; N, 13.60 Calc. for $C_{26}H_{42}N_4$: C, 76.09; H, 10.24; N, 13.66. Haai-$C_{18}H_{37}$ (**5a**), 59˚C ± 1˚C, *Anal.* Found: C, 76.50; H, 10.35; N, 13.30. Calc. for $C_{27}H_{44}N_4$: C, 76.42; H, 10.38; N, 13.21. Meaai-$C_{18}H_{37}$ (**5b**), 56˚C ± 1˚C, *Anal.* Found: C, 76.80; H, 10.55; N, 12.72 Calc. for $C_{28}H_{46}N_4$: C, 76.71; H, 10.50; N, 12.79. Haai-$C_{20}H_{41}$ (**6a**), 65˚C ± 1˚C, *Anal.* Found: C, 76.94; H, 10.66; N, 12.30 Calc. for $C_{29}H_{48}N_4$: C, 76.99; H, 10.62; N, 12.39. Meaai-$C_{20}H_{41}$ (**6b**), 63˚C ± 1˚C, *Anal.* Found: C, 77.31; H, 10.76; N, 12.06 Calc. for $C_{30}H_{50}N_4$: C, 77.25; H, 10.73; N, 12.02. Haai-$C_{22}H_{45}$ (**7a**), 65˚C ± 1˚C, *Anal.* Found: C, 77.60; H, 10.86; N, 11.70 Calc. for $C_{31}H_{52}N_4$: C, 77.51; H, 10.83; N, 11.67. Meaai-$C_{22}H_{45}$ (**7b**), 63˚C ± 1˚C, *Anal.* Found: C, 77.80 H, 10.88; N, 11.30 Calc. for $C_{32}H_{54}N_4$: C, 77.73; H, 10.93; N, 11.34%.

2.4. X-Ray Diffraction Study

The crystallographic data are shown in **Table 1**. Suitable single crystal of Meaai-$C_{16}H_{33}$ (**4b**) was mounted on a Siemens CCD diffractometer equipped with graphite monochromated Mo-K_α (λ = 0.71073 Å) radiation. The unit cell parameters and crystal-orientation matrices were determined for two complexes by least squares refinements of all reflections. The intensity data were corrected for Lorentz and polarisation effects and an empirical absorption correction were also employed using the SAINT program. Data were collected applying the condition $I > 2\sigma(I)$. All these structures were solved by direct methods and followed by successive Fourier and difference Fourier syntheses. Full matrix least squares refinements on F^2 were carried out using SHELXL-97 with anisotropic displacement parameters for all non-hydrogen atoms. Hydrogen atoms were constrained to ride on the respective carbon or nitrogen atoms with an isotropic displacement parameters equal to 1.2 times the equivalent isotropic displacement of their parent atom in all cases. Complex neutral atom scattering factors were used throughout for all cases. All calculations were carried out using SHELXS 97 [35], SHELXL97 [36] and PLATON 99 [37].

2.5. Computational Study

The direction of the dipole of the compound **5a** was calculated by Density Functional Theory (DFT), which may determine the presence of dipolar interaction within the molecules. All calculations have been performed by the Chem3D (version 10) [38] with GAUSSIAN 03 Interface [39]. The first optimization was done by the MM2 method, and finally DFT was performed as stated earlier.

3. Results and Discussion

3.1. Synthesis and Formulation

1-Alkyl-2-(arylazo)imidazole (Raai-C_nH_{2n+1}) are synthesized by controlled alkylation of 2-(arylazo)imidazole (RaaiH) by adding alkyl halide ($C_nH_{2n+1}X$) in dry THF using NaH. RaaiH are synthesized by diazo reaction of aryldiazonium salt with imidazole at pH 7 (**Scheme 2**). Alkyl halides of varying carbon chain (C_{10} to C_{22}) are used to synthesize Raai-C_nH_{2n+1} (n = 10 ($C_{10}H_{21}$, **1**), 12 ($C_{12}H_{25}$, **2**), 14 ($C_{14}H_{29}$, **3**), 16 ($C_{16}H_{33}$, **4**), 18 ($C_{18}H_{37}$, **5**), 20 ($C_{20}H_{41}$, **6**), 22 ($C_{22}H_{45}$, **7**)). The compounds are purified by chromatographic separation in silica gel column using acetonitrile-benzene (8:2, v/v). The elemental composition is supported by microanalytical data and they are low melting solid (*vide Experimental section*).

3.2. Spectral Studies

A moderately intense stretching for ν(C=N) is observed at 1585 - 1615 and ν(N=N) at 1370 - 1374 cm^{-1} (**Table 2**).

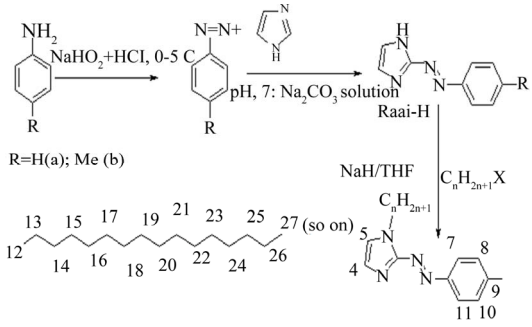

C_nH_{2n+1} n = 10 ($C_{10}H_{21}$, **1**), 12 ($C_{12}H_{25}$, **2**), 14 ($C_{14}H_{29}$, **3**), 16 ($C_{16}H_{33}$, **4**), 18 ($C_{18}H_{37}$, **5**), 20 ($C_{20}H_{41}$, **6**), 22 ($C_{22}H_{45}$, **7**)

Scheme 2. Synthetic process of Raai-C_nH_{2n+1} (1 - 7).

Table 1. Summarized crystallographic data for Meaai-$C_{16}H_{33}$ (4b).

	4b
Empirical formula	$C_{26}H_{42}N_4$
Formula weight	410.64
Temperature (K)	296
Crystal system	Monoclinic
Space group	P21/c
Crystal size $(mm)^3$	0.10 × 0.35 × 0.40
a(Å)	24.405(6)
b(Å)	11.049(3)
c(Å)	9.927(3)
β(°)	93.179(7)
V$(Å)^3$	2672.7(13)
Z	4
μ (MoK_α) (mm^{-1})	0.060
θ range	1.7 - 25.1
hkl range	−29 < h < 28; −13 < k < 12; −8 < l < 11
D_{calc} ($mg·m^{-3}$)	1.020
Refine parameters	273
Total reflections	15,392
Unique reflections	4696
R_1[a] [I > 2σ(I)]	0.0647
wR_2[b]	0.1409
Goodness of fit	1.039

[a]$R = \Sigma||F_o|-|F_c||/\Sigma|F_o|$; [b]$wR_2 = [\Sigma w(F_o^2-F_c^2)^2/\Sigma w(F_o^2)^2]^{1/2}$, $w = 1/[\sigma^2(F_0)^2 + (0.0986P)^2]$ for **4b**; where $P = (F_0^2 2^2 + 2Fc^2 2^2)/3$.

The stretching frequency of –N=N- (exocylic) are insignificantly affected on comparing with –C=N- (imidazolyl) group. This may support effect of alkylation at N(1)-imidazolyl position of the compounds [27].

The absorption spectra of the compounds were recorded in MeOH solution in the wavelength range 200 - 900 nm (**Figure 1**, **Table 2**). The absorption spectra of Raai-C_nH_{2n+1} show main absorption band at 355 - 375 nm with a molar absorption coefficient in the order of 10^4 $M^{-1}·cm^2$ and a weak band at 260 - 280 nm and 450 - 455 nm. The intense absorption band corresponds to π-π* transitions, while the tail portion is due to n-π* transition. With increasing chain length the absorption maxima have been shifted to longer wavelength which supports the enhancement of inductive effect of substituent with increase in number of bonded carbon centres at N(1)-imidazolyl group. The –N=N- is a part of a conjugated system of double bonds, both the **n**→π* and the π→π* bands are shifted to longer wavelength [40].

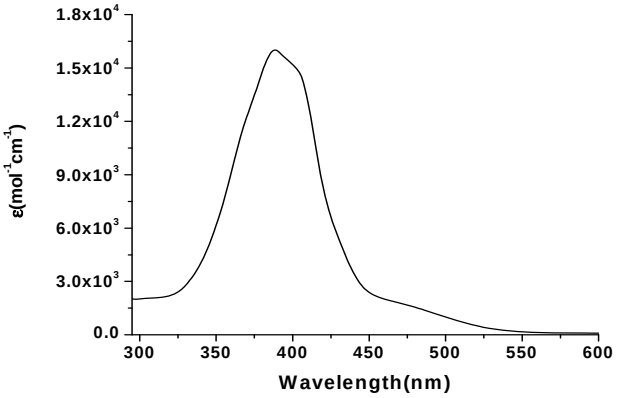

Figure 1. UV-Vis spectrum of Haai-$C_{20}H_{41}$ (6a) in methanol.

The ^1H NMR spectra of Raai-C_nH_{2n+1} (**1-7**) are recorded in $CDCl_3$. The atom numbering is shown in **Scheme 2**. The spectral data are set out in **Table 3**. The proton signals are assigned on the basis of spin-spin interaction and effect of substitution. The alkylation of imidazole is supported by the disappearance of δ(N–H) at ~10.30 ppm and the appearance of 1-alkyl signal at 0.85 - 4.40 ppm for -N–CH_2–(CH_2)n–CH_3. A triplet signal for -N–CH_2– appears at 4.40 ppm; and multiplet is observed for –(CH_2)n– at 0.80 - 1.50 ppm. Imidazolyl 4- and 5-H appear as broad singlet at 7.24 - 7.28 and 7.14 - 7.17 ppm, respectively. Broadening may be due to rapid proton exchange between these imidazolic protons. The aryl protons (7-H to 11-H) are upfield shifted on going from phenylazo (**a**) to *p*-tolylazo (**b**) which may be due to +I effect of –Me group.

3.3. Molecular Structure

The molecular structure of Meaai-$C_{16}H_{33}$ (**4b**) is shown in **Figure 2**. The bond parameters are listed in **Table 4**. The bond length and angles of the fragment of the structure, (*p*-tolylazo)imidazole, are comparable to the reported structure of Haai-Me [27]. The azo N-N distance is 1.266(4) Å which is slightly longer than the reported value (1.257(6) Å) [27]. Two groups around N=N are not perfectly planar and the dihedral angle between the two least squares planes is *avg*. 32°. The crowding of long chain, 1-$C_{16}H_{33}$ may be the reason for deviation. The

Table 2. FT-IR[a] and UV-VIS[b] spectral data of the compounds.

Compounds	IR in KBr disc (cm^{-1})		UV-Vis spectral data λ_{max}(nm), ($10^{-3} \in$ ($dm^3 \cdot mol^{-1} \cdot cm^{-1}$))
	ν(N=N)	ν(C=N)	
Haai-$C_{10}H_{21}$ (1a)	1403	1624	362 (25.9), 374 (24.1), 451 (2.4)
Meaai-$C_{10}H_{21}$ (1b)	1404	1625	363 (25.9), 376 (22.9), 451(2.1)
Haai-$C_{12}H_{25}$ (2a)	1404	1624	363 (27.1), 372 (23.9), 451(2.3)
Meaai-$C_{12}H_{25}$ (2b)	1405	1623	364 (28.9), 376 (22.9) ,452 (2.3)
Haai-$C_{14}H_{29}$ (3a)	1403	1624	365 (25.2), 376 (24.2), 454 (2.1)
Meaai-$C_{14}H_{29}$ (3b)	1403	1625	364 (26.9), 375 (23.6), 455 (2.2)
Haai-$C_{16}H_{33}$ (4[a])	1404	1624	365 (26.2), 375 (24.1), 451 (2.4)
Meaai-$C_{16}H_{33}$ (4b)	1404	1625	367 (25.9), 377 (24.5), 453 (2.1)
Haai-$C_{18}H_{37}$ (5a)	1405	1623	367 (25.8), 378 (24.2), 454 (2.1)
Meaai-$C_{18}H_{37}$ (5b)	1405	1625	368 (26.9), 378 (26.1), 455 (2.2)
Haai-$C_{20}H_{41}$ (6a)	1404	1624	370 (25.2), 380 (22.1), 458 (2.4)
Meaai-$C_{20}H_{41}$ (6b)	1405	1624	372 (25.9), 385 (23.6), 460 (2.1)
Haai-$C_{22}H_{45}$ (7a)	1404	1622	373 (19.3), 386 (17.3), 460 (1.98)
Meaai-$C_{22}H_{45}$ (7b)	1406	1620	373 (2.3), 385 (29.2), 462 (3.6)

[a]In KBr disc; [b]In methanol.

Table 3. ^{1}H NMR spectral data in $CDCl_3$ at room temperature.

Compounds	4-H[s]	5-H[s]	7,11-H[d]	8,10-H	9-R[s]	12-CH_2[t]	–$(CH_2)_{n-1}$-CH_3[*]
Haai-$C_{10}H_{21}$ (**1a**)	7.35	7.16	7.97 (8.2)	7.45[m]	7.43	4.43 (6.7)	1.88 - 1.28
Meaai-$C_{10}H_{21}$ (**1b**)	7.32	7.15	7.88 (8.5)	7.28 (7.0)[d]	2.42	4.40 (6.4)	1.87 - 1.29
Haai-$C_{12}H_{25}$ (**2a**)	7.34	7.17	7.94 (8.0)	7.46[m]	7.43	4.44 (7.1)	1.88 - 1.34
Meaai-$C_{12}H_{25}$ (**2b**)	7.31	7.14	7.90 (7.5)	7.28 (7.0)[d]	2.44	4.40 (6.4)	1.86 - 1.23
Haai-$C_{14}H_{29}$ (**3a**)	7.34	7.17	7.96 (8.1)	7.47[m]	7.46	4.42 (6.6)	1.89 - 1.25
Meaai-$C_{14}H_{29}$ (**3b**)	7.33	7.14	7.89 (8.6)	7.27 (7.0)[d]	2.41	4.41 (7.0)	1.89 - 1.28
Haai-$C_{16}H_{33}$ (**4a**)	7.35	7.16	7.97 (8.0)	7.49[m]	7.49	4.42 (6.6)	1.90 - 1.25
Meaai-$C_{16}H_{33}$ (**4b**)	7.27	7.14	7.96 (7.8)	7.27 (7.4)[d]	2.44	4.43 (7.0)	1.70 - 1.22
Haai-$C_{18}H_{37}$ (**5a**)	7.36	7.17	7.97 (8.2)	7.50[m]	7.49	4.41 (7.0)	1.89 - 1.23
Meaai-$C_{18}H_{37}$ (**5b**)	7.31	7.14	7.88 (8.5)	7.26 (7.4)[d]	2.43	4.40 (7.2)	1.87 - 1.21
Haai-$C_{20}H_{41}$ (**6a**)	7.35	7.16	7.96 (8.1)	7.52[m]	7.51	4.41 (7.0)	1.88 - 1.24
Meaai-$C_{20}H_{21}$ (**6b**)	7.32	7.14	7.89 (8.6)	7.27 (7.0)[d]	2.41	4.43 (7.0)	1.89 - 1.21
Haai-$C_{22}H_{45}$ (**7a**)	7.36	7.16	7.97 (8.2)	7.53[m]	7.52	4.42 (6.6)	1.90 - 1.22
Meaai-$C_{22}H_{45}$ (**7b**)	7.27	7.14	7.88 (8.5)	7.26 (7.0)[d]	2.41	4.40 (7.2)	1.86 - 1.22

[s]Singlet; [d]Doublet; [t]Triplet; [bs]Broad Singlet; [m] Multiplet; [*]protons of –$(CH_2)_{n-1}$-CH_3.

Table 4. Selected bond distances (Å) and angles (˚) for Meaai-$C_{16}H_{33}$ (4b).

Bond distances (Å)		Bond angles (˚)	
N(2)-C(1)	1.369(4)	C(12)-C(13)-C(14)	116.1(4)
N (2)-C(3)	1.352(50)	C(13)-C(14)-C(15)	117.4(4)
C(2)-C(3)	1.365(5)	C(23)-C(24)-C(25)	120.7(8)
N(1)-C(2)	1.356(4)	C(24)-C(25)-C(26)	119.8(9)
N(3)-C(1)	1.384(5)		
N(4-N(3)	1.262(4)		
N(4)-C(4)			

bonding strength between N and *p*-tolyl-C [C(8)–N(2), 1.421(4) Å] is weaker than that of N and imidazolyl-C [C(1)–N(1), 1.385(4) Å]. This suggests that the intramolecular interaction between azo-N and imidazolyl-C wave functions is stronger than that of *p*-tolyl orbitals. The C(3)-C(4) bond length (1.364(5) Å) of imidazolyl group is somewhat greater than reported data [41] which may be due to the steric demand of 1-$C_{16}H_{33}$ appended to imidazolyl group. The bond angle values at chain of C(15)-C(16)-C(17) (116.3(4)˚) C(20)-C(21)-C(22) (120.6 (6)˚), C(24)-C(25)-C(26) (123.6(8)˚) etc. show gradual increment which may be due to the removal of steric strain from the neighboring groups arranged in a zigzag manner. The imidazolyl-N is hydrogen bonded, N(3)---H(3)-C(3), (N(3)---H(3), 2.51 Å; N(3)---C(3), 3.390(5) Å and ∠ N(3)---H(3)-C(3), 158˚; symmetry, -x, -1/2+y, 1/2-z) to imidazolyl-C-H giving 1D chain (**Figure 3**). Packing view in the unit cell shows π---π interaction (3.3477(16) Å; symmetry, 1-x, 2-y, -z) between adjacent imidazolyl groups to form 2D supramolecular structure (**Figure 4**).

3.4. Photochromism

The irradiation of UV light at λ_{max} to a MeOH solution of the ligands has shown the absorption spectral change (**Figure 5**). The intense peak at λ_{max} decreases, which is accompanied by a slight increase at the tail portion of the spectrum until a photostationary state (PSS-I) is reached. Subsequent irradiation at the newly appeared longer wavelength peak reverses the course of the reaction and the original spectrum is recovered up to a point, which is another photostationary state (PSS-II) under irradiation at the longer wavelength peak. The quantum yields of the E-to-Z isomerisation were determined following previously reported procedure [26,27] and the results are set out in **Table 5**.

The absorption spectra of the E-isomer of ligands have changed with isosbestic points upon excitation (**Figure 5**) to the Z-isomer. The ligands show little sign of degradation upon repeated irradiation (**Figure 5(b)**). The quantum yields were measured for the E-to-Z ($\phi_{E\rightarrow Z}$) photoisomerisation of these ligands in MeOH. The $\phi_{E\rightarrow Z}$ values are significantly dependent on nature of substituents, and chain length of -C_nH_{2n+1}. The Me substituent, Haai-C_nH_{2n+1} to Meaai-C_nH_{2n+1}, and the alkyl substituent C_nH_{2n+1} (n = 10, 12, 14, 16, 18, 20, 22) at N(1)-position reduce $\phi_{E\rightarrow Z}$ values. In general, increase in mass of the molecule reduces the rate of isomerisation, E-to-Z. The rotor volume and mass have significant influence on the

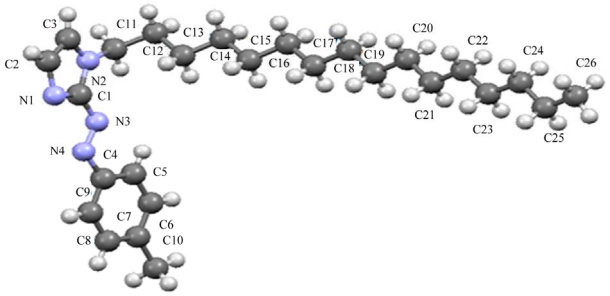

Figure 2. Crystal structure of Meaai-$C_{16}H_{33}$ (4b).

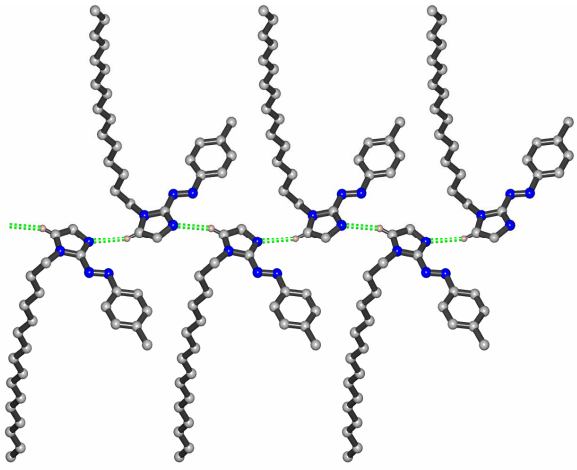

Figure 3. 1D supramolecular chains are formed along crystallographic b-axis through hydrogen bonding interactions of Meaai-$C_{16}H_{33}$ (4b).

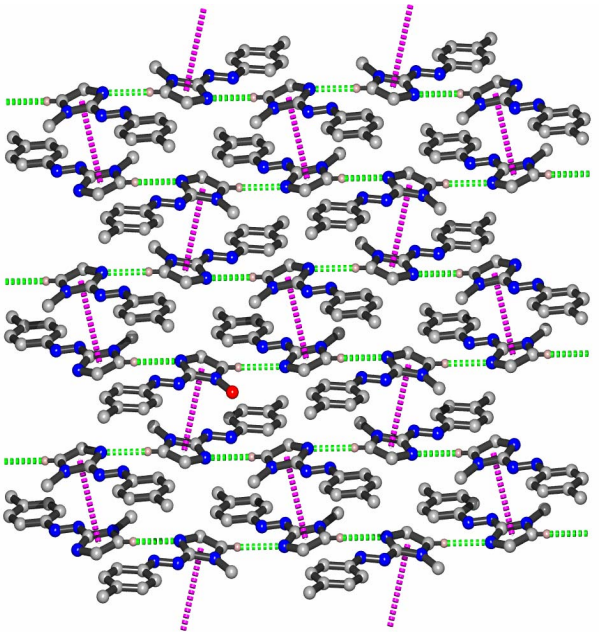

Figure 4. 2D supramolecular structure of Meaai-$C_{16}H_{33}$ (4b) formed by hydrogen bonding (Green) and π---π (magenta) interactions (for clarity the long aliphatic chains started from C15 (Red in color) and hydrogen atoms are not given).

isomerisation rate and quantum yields.

Thermal Z-to-E isomerisation of the ligands was followed by UV-Vis spectroscopy in MeOH at 298 - 313 K (**Table 6**). The Eyring plots in the range 298 - 313 K gave a linear graph from which the activation energy was obtained (**Table 6**, **Figure 6**). With the increase of the alkyl chain length on N atom of the imidazole moiety, the E_as are reduced which means faster Z-to-E thermal isomerisation. The entropy of activation (ΔS^*) are high negative in the organic compounds having large alkyl groups than that of the compounds having short alkyl chain. This is also in support of increase in rotor volume in the organic fragments.

3.5. Liquid Crystal Behaviour and Tansition Enthalpies of Haai-C_nH_{2n+1} (n = 18 (5a) and 22 (7a))

The thermal properties of the compounds were studied using polarized light optical microscopy (POM) and differential scanning calorimetry (DSC). Out of fourteen compounds only two compounds, Haai-$C_{18}H_{37}$ (**5a**) and Haai-$C_{22}H_{45}$ (**7a**) show mesomorphic response. The sample is sandwiched between untreated slide and a coverslip and is under hot stage of POM. Other twelve compounds show common crystalline-isotropic transition and the DSC plots do not show significant changes. The compound, **5a** exhibits nematic (N) texture at 55˚C (**Figure 7**) while **7a** shows unknown Smectic (Sm) phase at 62˚C (**Figure 8**) and, finally shift to isotropic (I) phase at 58˚C (**5a**) and 65˚C (**7a**) respectively. The crystal and nematic phases are under thermal equilibrium. During cooling from isotropic phase, **5a** shows strongly fluctuating textures of the N phase and has been transformed to textures in which "Schlieren" regions can be seen (**Figure 7**). Homeotropic and homogenous oriented domains cause this coexistence, which permits the assignment of the smectic phase in compound **7a**. The transition temperature and associated enthalpies are Cr → N 37.4˚C (15.9 KJ·mol^{-1}) → Iso 58˚C (0.5 KJ·mol^{-1}/heating cycle) → N 44.1˚C (12.6 KJ·mol^{-1}/cooling cycle) for **5a (Figure 9)**.

3.6. Computational Study

The Density Functional Theory (DFT) computation has been used to calculate dipole moment of **5a** and **7a**. It

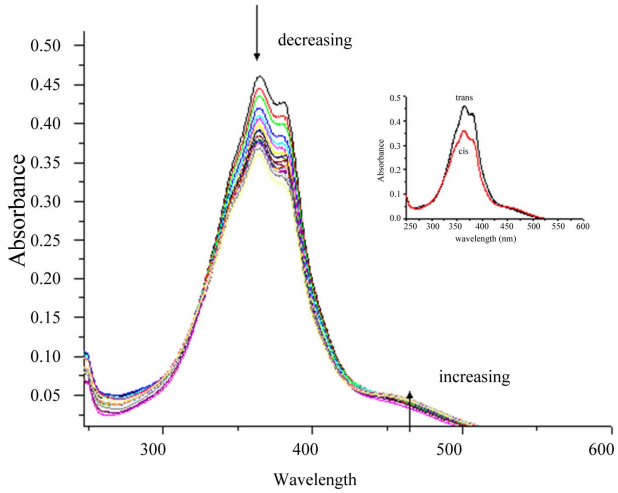

(a)

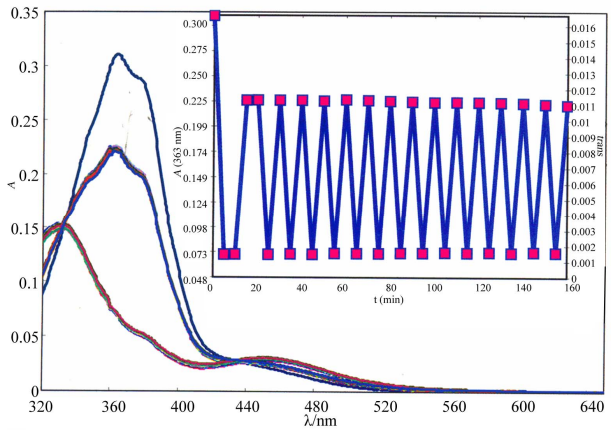

(b)

Figure 5. (a) Spectral changes of Haai-$C_{16}H_{33}$ (4a) in MeOH upon repeated irradiation at 365 nm at 3 min interval at 25˚C. Inset figure shows the spectra of Z and E isomers of Haai-$C_{16}H_{33}$; (b) Resistance to repeated irradiation in MeOH solution of Haai-$C_{16}H_{33}$ (4a).

Table 5. Results of photochromism, rate of conversion and quantum yields upon UV light irradiation.

Compounds	λ_{π,π^*} (nm)	Isobestic point (nm)	Rate of E→Z conversion × 10^9 (s^{-1})	$\phi_{E\to Z}$ Conversion × 10^9
Haai-$C_{10}H_{21}$ (**1a**)	362	328, 424	34.11	1.61
Meaai-$C_{10}H_{21}$ (**1b**)	363	326, 425	33.12	1.43
Haai-$C_{12}H_{25}$ (**2a**)	363	330, 427	32.76	1.54
Meaai-$C_{12}H_{25}$ (**2b**)	364	334, 425	32.14	1.38
Haai-$C_{14}H_{29}$ (**3a**)	361	326, 426	28.31	1.47
Meaai-$C_{14}H_{29}$ (**3b**)	361	328, 425	26.14	1.35
Haai-$C_{16}H_{33}$ (**4a**)	360	323, 432	25.81	1.37
Meaai-$C_{16}H_{33}$ (**4b**)	362	318, 436	24.80	1.29
Haai-$C_{18}H_{37}$ (**5a**)	362	315, 435	23.24	1.27
Meaai-$C_{18}H_{37}$ (**5b**)	363	312, 432	22.71	1.24
Haai-$C_{20}H_{41}$ (**6a**)	361	318, 429	22.13	1.20
Meaai-$C_{20}H_{21}$ (**6b**)	362	313, 445	21.14	1.19
Haai-$C_{22}H_{45}$ (**7a**)	360	319, 433	20.72	1.17
Meaai-$C_{22}H_{45}$ (**7b**)	363	311, 446	20.17	1.11

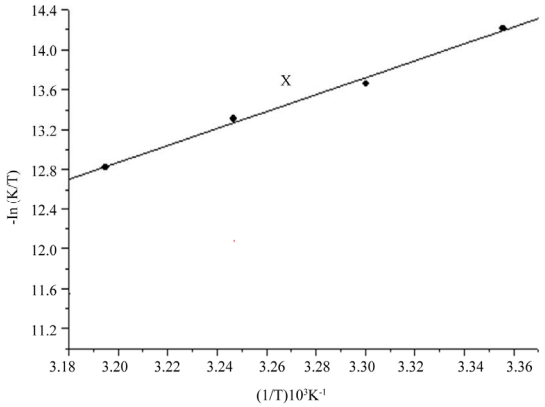

Figure 6. The Eyring plot of rate constants of Z-to-E thermal isomerisation of Haai-$C_{16}H_{33}$ (4a).

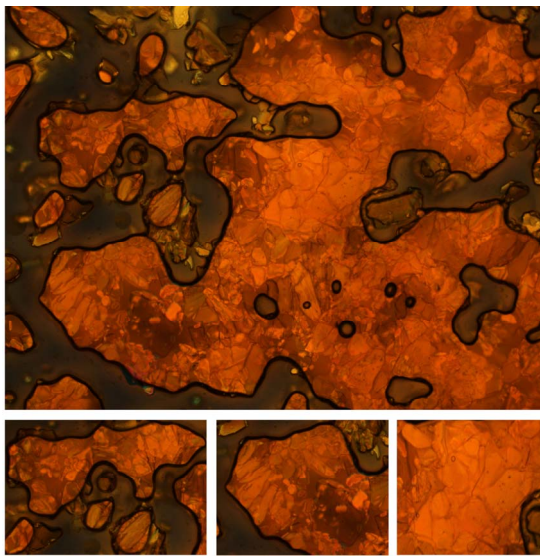

Figure 7. Fluctuating texture with schlieren texture of N phase at 51.2˚C of Haai-$C_{18}H_{37}$ (5a).

may determine the presence of dipolar interaction within the molecules (**Figure 10**). The dipole moment of **5a** is 2.997 Debye (X = −1.3726, Y = −2.4777, Z = 0.9814). After geometry optimization of the compound **5a** by addition of atoms step by step, the optimized structure suggests that the molecule possess rod shape. The first optimization was done by the MM2 method, and finally DFT was performed. The maxima of dipole moment are in the negative Y-direction (−2.4777 D), so the direction of net dipole moment should be along the molecular axis (axial). Therefore, the direction of net dipole moment is axial (along molecular axis). Near-neighbor antiparallel correlation of molecules within the layer of N phase will occur in reality if the direction of dipole is axial or along the molecular axis. The direction of rod shaped compound, **5a** in adjacent layers should be antiparallel, so that the layer polarization alternates from layer to layer; leading to a macroscopic apolar antiferroelectric structure which is applicable to N phases and sometime in case of reentrant Smectic phase with switching behavior. Within the layers the molecules are in most cases additionally non-tilted parallel to the polar direction in the case of the Nematic phase. DFT study suggests that the near-neighbour antiparallel correlation exists and in broad-on side position with respect to the direction of dipole within the layers. Based on the direction of the dipole moment, calculated from DFT we have constructed a model of supramolecular arrangement in Nematic phase which is depicted in **Figure 11**.

4. Conclusion

Seven pairs of 1-alkyl-2-(arylazo)imidazoles, Raai-C_nH_{2n+1} (n = 10, 12, 14, 16, 18, 20, 22) with long alkyl chain at imidazolyl-N(1) centre are spectroscopically

Table 6. Rate and activation parameters for Z (cis) → *E* (trans) thermal isomerisation.

Compounds	Temp (K)	Rate of thermal Z→E conversion × 10^3 (s^{-1})	E_a kJ mol^{-1}	ΔH^* kJ·mol^{-1}	ΔS^* J·mol^{-1}·K^{-1}	ΔG^* °kJ·mol^{-1}
Haai-$C_{10}H_{21}$ (**1a**)	298	0.2292	71.67	69.48	−81.94	92.14
	303	0.3898				
	308	0.5496				
	313	0.8867				
Meaai-$C_{10}H_{21}$ (**1b**)	298	0.2345	70.19	70.13	−83.47	90.12
	303	0.3976				
	308	0.5634				
	313	0.8979				
Haai-$C_{12}H_{25}$ (**2a**)	298	0.2367	69.86	68.97	−82.94	91.75
	303	0.3997				
	308	0.5645				
	313	0.8997				
Meaai-$C_{12}H_{25}$ (**2b**)	298	0.2654	69.06	68.89	−84.47	89.97
	303	0.4235				
	308	0.6167				
	313	0.9546				
Haai-$C_{14}H_{29}$ (**3a**)	298	0.2567	67.38	67.78	−84.49	90.34
	303	0.4135				
	308	0.5896				
	313	0.9123				
Meaai-$C_{14}H_{29}$ (**3b**)	298	0.2657	67.78	69.59	−86.67	86.67
	303	0.4767				
	308	0.6578				
	313	0.9545				
Haai-$C_{16}H_{33}$ (**4a**)	298	0.2789	65.34	67.73	−85.69	89.37
	303	0.4567				
	308	0.6189				
	313	1.0989				
Meaai-$C_{16}H_{33}$ (**4b**)	298	0.2577	73.40	70.85	−76.45	94.02
	303	0.4247				
	308	0.6276				
	313	0.9571				
Haai-$C_{18}H_{37}$ (**5a**)	298	0.3467	62.21	63.32	−87.79	87.79
	303	0.5567				
	308	0.7567				
	313	1.4567				
Meaai-$C_{18}H_{37}$ (**5b**)	298	0.4534	62.08	70.56	−89.97	85.54
	303	0.6989				
	308	0.8998				
	313	1.9675				
Haai-$C_{20}H_{41}$ (**6a**)	298	0.4569	60.45	61.89	−91.9	85.67
	303	0.6789				
	308	0.8765				
	313	1.9876				
Meaai-$C_{20}H_{21}$ (**6b**)	298	0.6578	60.09	69.99	−92.45	82.23
	303	0.7568				
	308	0.9678				
	313	2.1434				
Haai-$C_{22}H_{45}$ (**7a**)	298	0.4817	58.64	60.89	−92.38	83.45
	303	0.7541				
	308	0.9574				
	313	2.4270				
Meaai-$C_{22}H_{45}$ (**7b**)	298	0.7140	58.97	78.27	−43.90	91.56
	303	0.9247				
	308	1.2613				
	313	3.729				

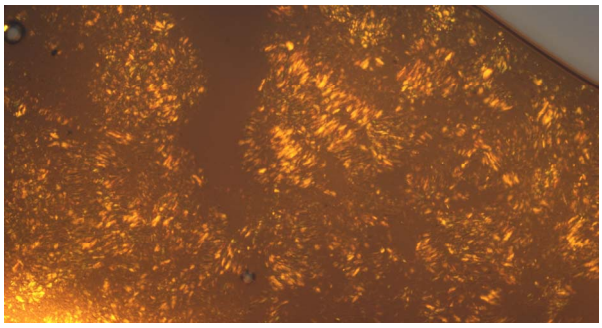

Figure 8. Unknown texture of Sm phase at 62˚C of Haai-$C_{22}H_{43}$.

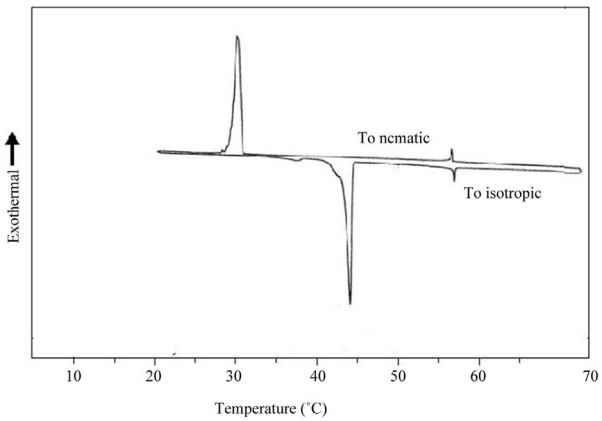

Figrue 9. DSC of Haai-$C_{18}H_{37}$ (5a) at the rate of 2˚C·min^{-1}.

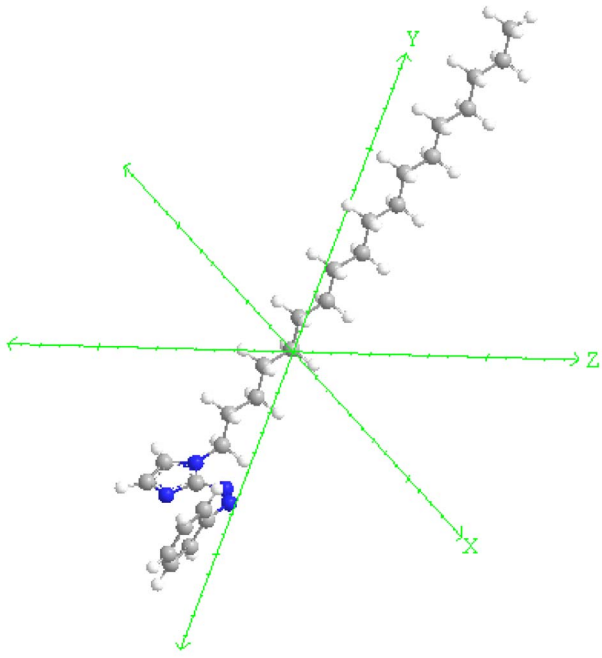

Figure 10. Optimized structure of compound 5a using DFT (B3LYP) level of theory.

characterised. As one of the compounds, 1-hexadcayl-2-(*p*-tolylazo)imidazole, Meaai-$C_{16}H_{33}$ is characterised by single crystal X-ray diffraction study. Upon UV light irradiation, the compounds show photochromism through geometrical isomerisation, E (trans)-to-Z (cis) forms. The reverse process is followed by thermal route and potential energy barrier (E_a) is calculated. The presence of long chain alkyl group shows long-range orientational order in between solid (crystalline, Cr) and isotropic (I) liquid phases. In some cases Cr and Nematic (N) texture shows thermal equilibrium in heating/cooling cycle. The Schlieren texture of N phase observed in compound **5a** and **7a** exhibits unknown smectic pahse with symmetrical lines. This is a preliminary report of our work; 1, 3-dialkyl-2-(arylazo)imida-zolium salts of different anions and the metal complexes (transition and nontransition) are waiting in this series.

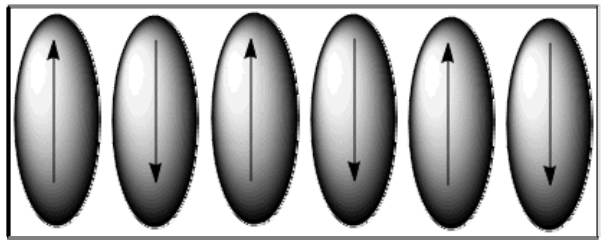

Figure 11. Schematic representation of supramolecular arrangement of dipoles in Nematic phase.

5. Acknowledgements

The authors express their sincere thanks to Department of Science and Technology, New Delhi for financial support. One of the authors (AN) thanks UGC for the award of Fellowship.

REFERENCES

[1] R. B. Wesley and B. L. Feringa, "Light Switching of Molecules on Surfaces," *Annual Reviews*: *Physical Chemistry*, Vol. 60, 2009, pp. 407-428. doi:10.1146/annurev.physchem.040808.090423

[2] N. L. Abbott, C. B. Gorman and G. M. Whitesides, "Active Control of Wetting Using Applied Electrical Potentials and Self-Assembled Monolayers," *Langmuir*, Vol. 11, No. 1, 1995, pp. 16-18. doi:10.1021/la00001a005

[3] L. Mu, Y. Liu, S. Y. Cai and J. L. Kong, "A Smart Surface in a Microfluidic Chip for Controlled Protein Separation," *Chemistry—A European Journal*, Vol. 13, No. 18, 2007, pp. 5113-5120. doi:10.1002/chem.200601624

[4] E. Katz, A. N. Shipway and I. Willner, "Electronic and Optical Transduction of Photoisomerization Processes at Molecular- and Biomolecular-Functionalized Surfaces," In: Z. Sekkat and W. Knoll, Eds., *Photoreactive Organic Films*, Academic, San Diego, 2002, pp. 220-268.

[5] M. Ire, "Photochromism: Memories and Switches—Introduction," *Chemical Reviews*, Vol. 100, No. 5, 2000, pp. 1683-1684. doi:10.1021/cr9800681

[6] S. Kawata and Y. Kawata, "Three-Dimensional Optical Data Storage Using Photochromic Materials," *Chemical Reviews*, Vol. 100, No. 5, 2000, pp. 1777-1788. doi:10.1021/cr980073p

[7] H. Dürr and H. Bouas-Laurent, "Photochromism: Molecules and Systems," Elsevier, Amsterdam, 2003.

[8] B. L. Feringa, "Molecular Switches," Wiley-VCH, Weinheim, 2001.

[9] J. C. Crano and R. J. Guglielmetti, "Organic Photochromic and Thermochromic Compounds," Kluwer Academic/ Plenum Publishers, New York, 1999.

[10] A. V. El'tsov, "Organic Photochromes," Consultants Bureau, New York, 1990.

[11] S. Furumi, H. Fudouzi and T. Sawada, "Dynamic Photoswitching of Micropatterned Lasing in Colloidal Crystals by the Photochromic Reaction," *Journal of Materials Chemistry*, Vol. 22, No. 40, 2012, pp. 21519-21528. doi:10.1039/c2jm34747d

[12] S. Pu, T. Wang, G. Liu, W. Liu and S. Cui, "A New Photoinduced Fluorescent Switch Based on a Photochromic Diarylethene with a Rhodamine Fluorophore," *Dyes and Pigments*, Vol. 94, No. 3, 2012, pp. 416-422. doi:10.1016/j.dyepig.2012.02.012

[13] M. Irie, "Special Issue Photochromism: Memories and Switches," *Chemical Reviews*, Vol. 100, No. 5, 2000, pp. 1683-1716. doi:10.1021/cr9800681

[14] S. Kobatake, S. Takami, H. Muto, T. Ishikawa and M. Irie, "Rapid and Reversible Shape Changes of Molecular Crystals on Photoirradiation," *Nature*, Vol. 446, No. 7137, 2007, pp. 778-781. doi:10.1038/nature05669

[15] T. L. Andrew, H. Y. Tsai and R. Menon, "Confining Light to Deep Subwavelength Dimensions to Enable Optical Nanopatterning," *Science*, Vol. 324, No. 5929, 2009, pp. 917-921. doi:10.1126/science.1167704

[16] H. Bouas-Laurent and H. Dürr, "Organic Photochromism," *Pure and Applied Chemistry*, Vol. 73, No. 4, 2001, pp. 639-665. doi:10.1351/pac200173040639

[17] C. V. Yelamaggad, I. Shashikala, U. S. Hiremath, D. S. S. Rao and S. K. Prasad, "Liquid Crystal Dimers Possessing Chiral Rod-Like Anisometric Segments: Synthesis, Characterization and Electro-Optic Behavior," *Liquid Crystals*, Vol. 34, No. 2, 2007, pp. 153-167. doi:10.1080/02678290601137585

[18] P. M. Maitlis, A. Giroud-Godquin and M. Angecu, "Metallomesogens: Metal Complexes in Organized Fluid Phases," *Angewandte Chemie International Edition in English*, Vol. 30, No. 4, 1991, pp. 375-402 doi:10.1002/anie.199103751

[19] V. Balzani, "Molecular Devices and Machines," Wiley-VCH, Weinheim, 2008.

[20] S. Gerlich, L. Hackermüller, K. Hornberger, A. Stibor, H. Ulbricht, M. Gring, F. Goldfarb, T. Savas, M. Müri, M. Mayor and M. Arndt, "A Kapitza-Dirac-Talbot-Lau Interferometer for Highly Polarizable Molecules," *Nature Physics*, Vol. 3, No. 10, 2007, pp. 711-715. doi:10.1038/nphys701

[21] H. Hartmann and I. Zug, "On the Coupling of Aryldiazonium Salts with *N*,*N*-Disubstituted 2-Aminothiophenes and Some of Their Carbocyclic and Heterocyclic Analogues," *Journal of the Chemical Society*, *Perkin Transactions*, Vol. 1, No. 24, 2000, pp. 4316-4320. doi:10.1039/b006803i

[22] M. M. M. Raposo, A. M. R. C. Sousa, A. M. C. Fonseca and G. Kirsch, "Thienylpyrrole Azo Dyes: Synthesis, Solvatochromic and Electrochemical Properties," *Tetrahedron*, Vol. 61, No. 34, 2005, pp. 8249-8256. doi:10.1016/j.tet.2005.06.039

[23] B. A. Trofimov, E. Y. Schmidt, A. I. Mikhaleva, A. M. Vasiltsov, A. B. Zaitsev, N. S. Smolyanina, A. V. Afonin, I. A. Ushakov, K. B. Petrushenko, O. N. K. Kazheva, O. A. Dyachenko, V. V. Smirnov, A. F. Schmidt, M. V. Markova and L. V. Morozova, "2-Arylazo-1-vinylpyrroles: A Novel Promising Family of Reactive Dyes," *European Journal of Organic Chemistry*, Vol. 2006, No. 17, 2006, pp. 4021-4033. doi:10.1002/ejoc.200600357

[24] P. J. Coelho, M. C. R. Castro, A. M. C. Fonseca and M. M. M. Raposo, "Photoswitching in Azo Dyes Bearing Thienylpyrrole and Benzothiazole Heterocyclic Systems," *Dyes and Pigments*, Vol. 92, No. 1, 2011, pp. 745-748. doi:10.1016/j.dyepig.2011.06.019

[25] U. Ray, D. Banerjee, G. Mostafa, T.-H. Lu and C. Sinha, "Copper Coordination Compounds of Chelating Imidazole-Azo-Aryl Ligand. The Molecular Structures of Bis[1-ethyl-2-(*p*-tolylazo)imidazole]-bis-(azido)copper(II) and Bis[1-methyl-2(phenylazo)imidazole]-bis(thiocyanato)copper(II)," *New Journal of Chemistry*, Vol. 28, No. 12, 2004, pp. 1437-1442. doi:10.1039/b406445c

[26] J. Otsuki, K. Suwa, K. Narutaki, C. Sinha, I. Yoshikawa and K. Araki, "Photochromism of 2-(Phenylazo)imidazoles," *The Journal of Physical Chemistry A*, Vol. 109, No. 35, 2005, pp. 8064-8069. doi:10.1021/jp0531917

[27] J. Otsuki, K. Suwa, K. K. Sarker and C. Sinha, "Photoisomerization and Thermal Isomerization of Arylazoimidazoles," *The Journal of Physical Chemistry A*, Vol. 111, No. 8, 2007, pp. 1403-1409. doi:10.1021/jp066816p

[28] K. K. Sarker, A. D. Jana, G. Mostafa, J.-S. Wu, T.-H. Lu and C. Sinha, "Iodo Bridged Lead(II) Compounds of Azoimidazoles: Single Crystal X-Ray Structures of [Di-iodo-{1-methyl-2-(p-tolylazo)imidazole}lead(II)]$_n$ and {1-Methyl-3-benzyl-2-(p-tolylazo)imidazolium}$_m$-{tri-iodoplumbate(II)}$_m$," *Inorganica Chimica Acta*, Vol. 359, No. 13, 2006, pp. 4377-4385. doi:10.1016/j.ica.2006.05.037

[29] K. K. Sarker, D. Sardar, K. Suwa, J. Otsuki and C. Sinha, "Cadmium(II) Complexes of (Arylazo)imidazoles: Synthesis, Structure, Photochromism, and Density Functional Theory Calculation," *Inorganica Chemistry*, Vol. 46, No. 20, 2007, pp. 8291-8301. doi:10.1021/ic7012073

[30] K. K. Sarker, B. G. Chand, K. Suwa, J. Cheng, T.-H. Lu, J. Otsuki and C. Sinha, "Structural Studies and Photochromism of Mercury(II)-Iodo Complexes of Arylazoimidazoles," *Inorganica Chemistry*, Vol. 46, No. 3, 2007, pp. 670-680. doi:10.1021/ic061221u

[31] P. Pratihar, T. K. Mondal, A. K. Patra and C. Sinha, "*trans*-Dichloro-bis-(arylazoimidazole)palladium(II): Synthesis, Structure, Photoisomerization, and DFT Calculation," *Inorganica Chemistry*, Vol. 48, No. 7, 2009, pp. 2760-2769. doi:10.1021/ic8012365

[32] D. Demus, J. Goodby, G. W. Gray, H. W. Spiess and V. Vill, "Handbook of Liquid Crystals," Wiley-VCH, Weinheim, 1998.

[33] D. Demus, J. Goodby, G. W. Gray, H. W. Spiess and V. Vill, "Dunmur D and Toriyama K. Handbook of Liquid Crystals, Vol 1, Chapter VII," Wiley-VCH, Weinheim, 1998.

[34] K. Binnemans, "Ionic Liquid Crystals," *Chemical Reviews*, Vol. 105, No. 11, 2005, pp. 4148-4204. doi:10.1021/cr0400919

[35] G. M. Sheldrick, "SHELXS 97, Program for the Solution of Crystal Structure," University of Göttingen, Göttingen, 1990.

[36] G. M. Sheldrick, "SHELXL 97, Program for the Refinement of Crystal Structure," University of Göttingen, Göttingen, 1997.

[37] A. L. Spek, "Structure Validation in Chemical Crystallography," *Acta Crystallographica Section D*, Vol. 65, No. 2, 2009, pp. 148-155. doi:10.1107/S090744490804362X

[38] Cambridge Soft Corporation: USA, "Chem3D, Version 10," Cambridge Soft, Cambridge, 2006.

[39] M. J. Frisch, "GAUSSIAN 03 (Revision c.02)," Gaussian, Wallingford, 2004.

[40] M. M. Enriquez, M. Fuciman, A. M. LaFountain, N. L. Wagner, R. R. Birge and A. H. Frank, "The Intramolecular Charge Transfer State in Carbonyl-Containing Polyenes and Carotenoids," *The Journal of Physical Chemistry B*, Vol. 114, No. 38, 2010, pp. 12416-12426. doi:10.1021/jp106113h

[41] P. Bhunia, B. Baruri, U. S. Ray and C. Sinha, "Azoimidazole Complexes of Manganese(II)-Thiocyanate. X-Ray Structures of 2-(p-tolylazo)imidazole and Bis-[1-methyl-2-(p-tolylazo)imidazole]-di-thiocyanato-manganese(II)," *Transition Metal Chemistry*, Vol. 31, No. 3, 2006, pp. 310-315. doi:10.1007/s11243-005-6401-4

Supplementary Material

Crystallographic data for the structures have been deposited with the Cambridge Crystallographic Data Center; CCDC No. 854093. Copies of this information may be obtained free of charge from the Director, CCDC, 12 Union Road, Cambridge CB2 1EZ, UK (e-mail, deposit@ccdc.cam.ac.uk, or www, htpp://www.ccdc.cam.ac.uk).

